Effect of Deposition Rate on the Stress Evolution of Plasma-Sprayed Yttria-Stabilized Zirconia

Kentaro Shinoda, Jose Colmenares-Angulo, Alfredo Valarezo, and Sanjay Sampath

The deposition rate plays an important role in determining the thickness, stress state, and physical properties of plasma-sprayed coatings. In this article, the effect of the deposition rate on the stress evolution during the deposition (named evolving stress) of yttria-stabilized zirconia coatings was systematically studied by varying the powder feed rate and the robot-scanning speed. The evolving stress during the deposition tends to increase with the increased deposition rate, and this tendency was less significant at a longer spray distance. In some cases, the powder feed rate had more significant influence on the evolving stress than the robot speed. This tendency can be associated with a deviation of a local deposition temperature at a place where sprayed particles are deposited from an average substrate temperature. At a further higher deposition rate, the evolving stress was relieved by introduction of macroscopic vertical cracks as well as horizontal branching cracks.

1. Introduction

Plasma spraying is a versatile technology to produce relatively thick coatings up to a few millimeters exhibiting a diverse range of microstructures. Typical applications of yttria-stabilized zirconia (YSZ) include highly porous abradable coatings, conventional (CON) layered thermal barrier coatings (TBCs), strain-tolerant TBCs with vertical cracks, and dense electrolytes for solid oxide fuel cells, all of which can be fabricated with a single plasma torch (Ref 1-3). Tailoring these microstructures requires control of porosity and crack architecture by process parameters. This control can be achieved by manipulating non-particle state parameters (NPSPs) such as the deposition temperature and the deposition rate in addition to particle state parameters (PSPs) such as the particle temperature and velocity (Ref 4). The development of in-flight particle diagnostics and advanced numerical simulations has enabled the quantitative study of the effects of the PSPs on coating microstructures (Ref 5-9). However, in contrast to the PSPs, lack of in situ diagnostic tools for the NPSPs

has hindered a systematic study on the NPSPs. Recent developments in robust in situ curvature monitoring during thermal spraying along with analytical tools to extract linear and nonlinear elastic properties (Ref 8, 10-13) give us an opportunity to enhance our understanding regarding the effects of NPSPs on stresses and coating architecture.

A process map method is an effective approach to correlate process input parameters with coating microstructures and properties, which are the result of variations of these input parameters in plasma spraying (Ref 2, 5, 8, 14). In the process map method, the process input parameters and the coating properties are correlated via PSPs with two-step process maps: the first-order process map is to link the process input parameters (namely, plasma forming gas mass flow rate, primary/secondary gas ratio, and current) with the PSPs such as particle temperature and velocity; the second-order process map to link the PSPs and the coating properties (such as thermal conductivity and modulus of the coatings). This methodology is also applicable to investigate the effects of the NPSPs, and will be applied to our research. Consideration of intrinsic NPSPs for the process map is also the subject of this article.

In representing the NPSPs, we focus on the deposition rate. Here, we use the mass of the powder injected per unit length as the deposition rate R_d, and thus it is described by

$$R_d = \frac{R_f}{U}, \tag{Eq 1}$$

where R_f is the powder feed rate and U is a relative speed between the plasma torch and the substrate (equal to the robot speed when the substrate is fixed). This term is also called an application rate or spray rate. As the powder feed rate is increased at constant power conditions, a possible consequence is reduction in average particle temperature and velocity due to quenching of the plasma plume. However, prior work by the authors has indicated

Kentaro Shinoda, Jose Colmenares-Angulo, Alfredo Valarezo, and **Sanjay Sampath**, Department of Materials Science and Engineering, Center for Thermal Spray Research, Stony Brook University (State University of New York at Stony Brook), 130 Heavy Engineering, Stony Brook, NY 11794-2275. Contact e-mail: kentaro.shinoda@aist.go.jp.

that such powder loading effects were not severe up to about the powder feed rate $R_f = 45$-60 g/min for standard plasma spray torches (~35 kW) with a single injector (Ref 4). For such a range of operating conditions, the deposition rate will be proportional to the thickness per pass of the coating. In addition, the deposition rate can affect thermal history during deposition and thus resultant stress evolutions (Ref 15). Therefore, the deposition rate is considered to be one of the important NPSPs to describe the deposition.

The stress state of a coating/substrate system can be described by three stresses and the resultant residual stress. The stress that can be accumulated during substrate preparation such as grit blasting is compressive. This compressive stress may be partially relieved by a heat input during the deposition (Ref 16). The second category is stress accumulated during the coating deposition. This stress is generally tensile for low velocity processes such as plasma spray, and was termed quenching stress by Kuroda and Clyne (Ref 10) and describes the stress arising due to constrained cooling of the deposited material. Valarezo et al. (Ref 17, 18) elaborated on this concept describing this quantity as an evolving stress so as to capture relaxation mechanisms as well as secondary factors such as peening effects in high velocity deposition. In plasma spraying, the evolving stress mainly consists of the tensile quenching stress, with partial relief due to microcracking at the single splat or multiple splat levels and splat sliding (Ref 10). Finally, thermal stress is caused by a thermal expansion mismatch between the coating and the substrate during cooling from a deposition temperature (Ref 19). Among these stresses, since the evolving stress represents the deposition of the coating, it will be a key factor to link the process conditions with coating properties.

In general, the evolving stress and coating modulus increased and the porosity of the coatings decreased with increased substrate temperature (Ref 20). Kuroda et al. (Ref 20) explained that improved wetting by the temperature increase caused better bonding of splats, resulting in a higher evolving stress. This improved bonding by increasing a substrate temperature was also confirmed by an increase in a coating elastic modulus when deposited at higher substrate temperatures (Ref 21). These studies suggest the importance of the deposition temperature on the stress evolution of a coating during deposition, which can be varied by the deposition rate.

In this article, we present a comprehensive set of experiments on the effect of the deposition rate on the stress evolution during the deposition of YSZ coatings by plasma spraying. An in situ curvature sensor is utilized to explore the NPSP effects systematically. In particular, the effects of the powder feed rate and the robot speed are examined by utilizing the process map method. The importance of local deposition rate and local deposition temperature is discussed.

2. Materials and Methods

An atmospheric dc plasma torch with an 8 mm diameter nozzle and a swirl flow gas distribution ring (F4-MB,

Sulzer Metco Inc., Westbury, NY, USA) was used in this study. Hollow spherical (HOSP) powder of 8 wt.% YSZ (10-75 µm) (#204, Saint-Gobain Ceramic Materials, MA, USA) was sprayed under a plasma condition shown in Table 1. The powder was injected through an external injector perpendicular to the spray axis. A constant plume depth method (Ref 22) was utilized for optimization of powder injection to increase the repeatability of the experiments. A single particle-type diagnostics system (DPV-2000, Tecnar Automation Ltd, Quebec, Canada) was used to monitor the plume depth and in-flight particle states such as temperature and velocity. The torch operating condition was kept constant, and only the robot-scanning speed U and the powder feed rate R_f were varied. Basically one set of the deposition rate experiment consisted of 12 combinations = 3 robot speeds ($U = 333$, 500, and 1000 mm/s) × 4 powder feed rates ($R_f = 15$, 30, 45, and 60 g/min), and additional runs were conducted if needed. As introduced in section 1, the powder feed rate was varied within a range where the powder loading effect was not severe. Note that decreases in particle temperature due to the powder loading effect at a constant power may be compensated by either an open loop or closed-loop control using a process map (Ref 6, 23). However, this adjustment was not conducted in this article, because changing a plasma torch operating condition will also change the heat flux from the plasma jet to the substrate, resulting in evoking other issues to be considered. In order to evaluate stress evolutions at further high deposition rates with keeping the powder loading effect minimized, a high-throughput (HTP) plasma torch (Triplex 200 Pro, Sulzer Metco, Westbury, NY, USA) was utilized. The input power of this torch was ~50 kW, much larger than that of the CON plasma torch used in this study (~34 kW).

The stress evolution during deposition was monitored by an in situ curvature method. An in situ coating property (ICP) sensor was utilized to monitor the curvature of a coating/substrate system as well as the substrate temperature. The principle of the ICP sensor is described elsewhere in detail (Ref 13), and briefly described here. Aluminum beams (Al6061-T6) of length $L = 228.6$ mm and width $W = 25.4$ mm were used as substrates. The thickness of the substrates was $h_s = 1.6$, 2.4, and 3.2 mm. Both edges of the substrate were mounted to the ICP sensor with springs. The displacement of the substrate at the center was monitored from the backside of the

Table 1   Plasma spray conditions

Process parameters	Values
Primary Ar gas flow rate (SLM)	47.5
Secondary H$_2$ gas flow rate (SLM)	6.0
Current, A	550
Power, kW	34
Cooling jet, psi	40
Spray distance, x, mm	100, 150
Robot speed, U, mm/s	250, 333, 500, 1000
Powder feed rate, R_f, g/min	15, 30, 45, 60

SLM, standard liters per minute

substrate with a laser displacement sensor having the resolution of 1 μm. The sampling rate was set to be 10 Hz. The curvature was calculated from the displacement. The substrate temperature was monitored simultaneously using two K-type thermocouples in contact with both sides of the substrate backside. Figure 1 shows a typical result of the curvature and substrate temperature evolutions during the deposition. A positive curvature change corresponds to a tensile stress in the coating. Here, we have introduced the concept of an evolving stress to evaluate the degree of a stress accumulated during the deposition. The evolving stress is defined as the gradient of the curvature evolution when the curvature change is linearly approximated. Thus, the evolving stress during the deposition, σ_{ev}, was calculated from the curvature data utilizing Stoney's formula as follows (Ref 8, 13, 17, 18, 24)

$$\sigma_{ev} = \frac{E_s h_s^2}{6(1-\nu_s)} \frac{\Delta\kappa}{\Delta h_c} \qquad \text{(Eq 2)}$$

where E_s, ν_s, $\Delta\kappa$, and Δh_c are the substrate Young's modulus, substrate Poisson's ratio, the curvature, and coating thickness change at a calculated region, respectively. The value of ν_s was set to 0.33 and E_s was temperature-dependent as follows (Ref 25) (Material Property Database, version 3.51, JAHM Software, Inc., North Reading, MA, USA):

$$E_s(T_s) = -2.65 \times 10^{-7} T_s^3 + 2.40 \times 10^{-4} T_s^2$$
$$- 9.21 \times 10^{-2} T_s + 85.2 \text{ (GPa)}$$
$$\text{for } 113\,\text{K} < T_s \le 573\,\text{K} \qquad \text{(Eq 3)}$$

$$E_s(T_s) = -1.73 \times 10^{-4} T_s^2 + 1.12 \times 10^{-1} T_s + 53.9 \text{ (GPa)}$$
$$\text{for } 573\,\text{K} < T_s \le 773\,\text{K} \qquad \text{(Eq 4)}$$

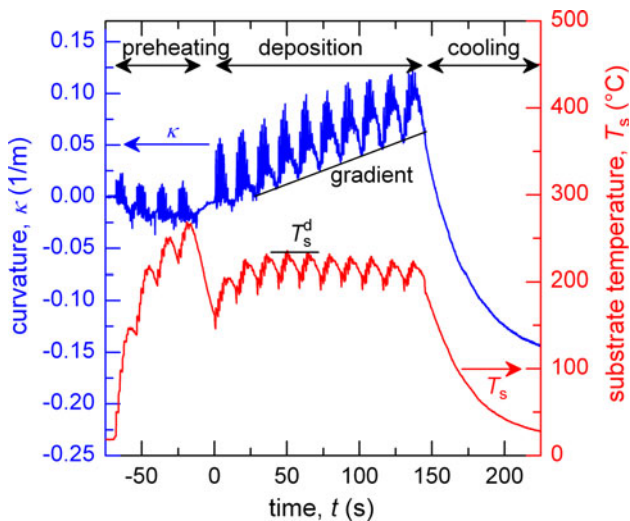The maximum substrate temperature during the deposition stage T_s^d was usually used as the substrate temperature

unless otherwise noted. The value of Δh_c was given by $\Delta h_c = h_c \Delta t_{cal}/t_d$, where h_c, Δt_{cal}, and t_d are the thickness of the coating measured *ex situ*, a period of time used for the calculation, and the total deposition time, respectively.

Our static test using a precise-temperature-controlled furnace coupled with a finite element method estimated the accuracy of the curvature measurement and the stress to be 1% and ± 3 MPa, respectively (Ref 26). During deposition, although thermal gradients through thickness and in plane can exist due to plasma and particle plumes (Ref 26, 27), their effects on $\Delta\kappa$ are not significant. This is because we measure real-time change in curvature and not the absolute value. Under steady state temperature, the temperature profile (albeit not uniform) at given time is similar between passes. This means that the temperature gradient effects are subtracted from pass to pass. Many recent studies also reported that Stoney's formula could eventually be applied to thick films, even though it was intended to be applied to thin films (Ref 28). Indeed for $h_s = 3.2$ mm and $h_c = 0.32$ mm, the moment inertia by a correct bimaterial formula was ~13% more than that estimated from Stoney's formula. However, for computing stress (Ref 26, 27), the difference was only 3-5%.

The cross section of the YSZ coatings was observed with a scanning electron microscope (SEM). The porosity of the coatings, ρ, was calculated from backscattered electron images of the cross sections obtained at a magnification of 2000 by an image analysis using a software (ImagePro Plus J6.1, Media Cybernetics, Bethesda, MD, USA). The deposition efficiency η was determined by a weight ratio of the coating to injected powder onto the substrate. The detailed definition can be found elsewhere (Ref 4).

3. Results

Figure 2 describes the evolving stress as a function of the deposition rate. In general, a higher deposition rate tends to have given a higher evolving stress. The evolving stress was lower when samples were deposited at a longer spray distance ($x = 150$ mm) compared to a CON spray distance ($x = 100$ mm). The dependence of the evolving stress on the deposition rate was also less significant at a longer spray distance.

Figure 3 shows the microstructure of the YSZ coatings at two spray distances ($x = 100$ and 150 mm) when the powder feed rate was varied. More pores were apparently observed at $x = 150$ mm (Fig. 3e, f) than at $x = 100$ mm (Fig. 3a to d). The porosity of the coatings quantitatively confirmed this tendency, as shown in Fig. 4(a). Although the porosity tends to have increased at the highest powder feed rate of $R_f = 60$ g/min, the effect of the powder loading on the porosity was not significant up to $R_f = 45$ g/min. Figure 4(b) shows the effect of the powder feed rate on the deposition efficiency of the coatings at two spray distances. No significant dependencies of the porosity and the deposition efficiency of the coatings on the robot speed were observed, so these values were averaged ones for different robot speeds. The deposition efficiency of
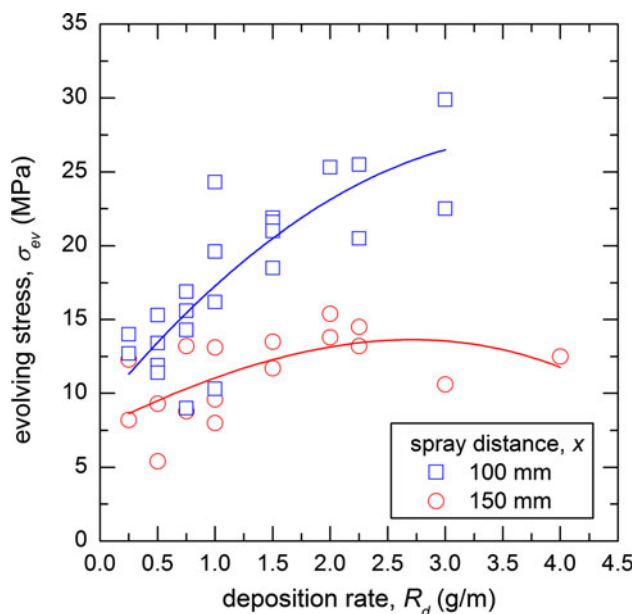

Fig. 1 Evolutions of substrate curvature κ and substrate temperature T_s during the deposition of an YSZ coating by plasma spraying. These evolutions are monitored with an ICP sensor. The maximum substrate temperature during the deposition stage, T_s^d is used as a representative of the substrate temperature (Color online)

Fig. 2 Effect of deposition rate R_d on evolving stress σ_{ev}. Two spray distances: standard ($x = 100$ mm) and a longer one ($x = 150$ mm) are examined. Hollow spherical powder of YSZ (10-75 μm) was sprayed onto Al beams 2.4 mm thick at 34 kW (Color online)

$x = 150$ mm was about half that of $x = 100$ mm. The deposition efficiency at $x = 100$ mm tends to have decreased slightly with the powder feed rate, while that at $x = 150$ mm was less dependent on it.

Figure 5 re-plotted the evolving stress shown in Fig. 2 against the substrate temperature. The evolving stress tends to have monotonically increased with the substrate temperature. This tendency suggests that the effect of the deposition rate on the stress evolution can be explained mainly by an increase of the substrate temperature with the deposition rate. Note that no distinct gap in the values of the evolving stresses can be found at the substrate temperature of ~250 °C between the spray distances of $x = 150$ mm and 100 mm in contrast to Fig. 2. This fact is somewhat surprising because the microstructure of the coatings sprayed at $x = 150$ mm clearly showed a higher porosity than those at $x = 100$ mm. The higher porosity could result in a further drop in the evolving stress, which might have lead to a gap in the data between two spray distances. Therefore, the effect of deposition temperature on the stress evolution is considerably large to hinder the effect of particle state change.

Figure 6 shows the effect of substrate thickness on the stress evolution. The evolving stress of thinner substrates had a steeper gradient against the deposition rate. A smaller heat content of substrates at thinner substrates was considered to be a primary reason for this fact.

In order to see the effect of the deposition rate in detail, the thickness per pass, the substrate temperature, and the evolving stress were plotted as a function of the powder feed rate and the inverse of the robot speed in the form of a two-dimensional map (Fig. 7). As the deposition

rate is given by a product of the powder feed rate and the inverse of the robot speed, the right top side of the figures corresponds to a higher deposition rate. As expected, the thickness per pass increased with the increased powder feed rate or with the decreased raster speed (Fig. 7a). Within the range of this study, the effects of the feed rate and the inverse of the robot speed were equivalent in terms of the thickness per pass. This fact does not conflict with a weak dependence of the deposition efficiency on the powder feed rate shown in Fig. 4. The substrate temperature also tends to have increased with the powder feed rate and the inverse of the robot speed (Fig. 7b). The robot speed had more influence on the substrate temperature than the powder feed rate. On the contrary, Fig. 7(c) shows that the powder feed rate had a more significant effect on the evolving stress compared to the robot speed. Since the substrate temperature also depends on other factors such as the geometry of the substrate and the robot-scanning program, the results shown above cannot be simply applied to all the cases, but in many cases, the powder feed rate seems to have more significant effect than the robot speed on the evolving stress, which will be further discussed in section 4.1.

At a further high deposition rate without a significant powder loading effect, the behavior of the stress evolution can be different from what was shown above. Figure 8 shows the evolving stress of YSZ coatings deposited with a HTP plasma torch. On the contrary to those with a CON plasma torch as discussed above, the evolving stress was not accumulated during deposition ($\sigma_{ev} \leq 5$ MPa) at a high deposition rate ($R_d = 4.5$ g/m). In such a coating, vertical cracks as well as horizontal branching cracks were observed, as shown in Fig. 9(a). Conversely, by decreasing the deposition rate via increasing the robot speed, cracks can be suppressed as shown in Fig. 9(b). Crack initiations are likely attributed to a high tensile stress during deposition at a high deposition rate.

4. Discussion

4.1 Local Deposition Temperature and Local Deposition Rate

Introduction of a local deposition temperature and a local deposition rate can be useful to explain the observed experimental results. According to Kuroda et al. (Ref 20), the higher the deposition temperature is, the higher the quenching stress is. Our results also generally followed this tendency. A better bonding of splat interfaces due to an enhanced wettability at a higher deposition temperature is considered to be responsible on this tendency (Ref 20, 29); therefore, the main source of the evolving stress came from the quenching stress as described in section 1. In plasma spraying, the coating formation is localized and dependent on the spray torch positioning, unlike other methods such as electron beam physical vapor deposition where the coating growth is more uniform. Deposit lines referred to as beads are formed by successive impact of individual particles, as shown in
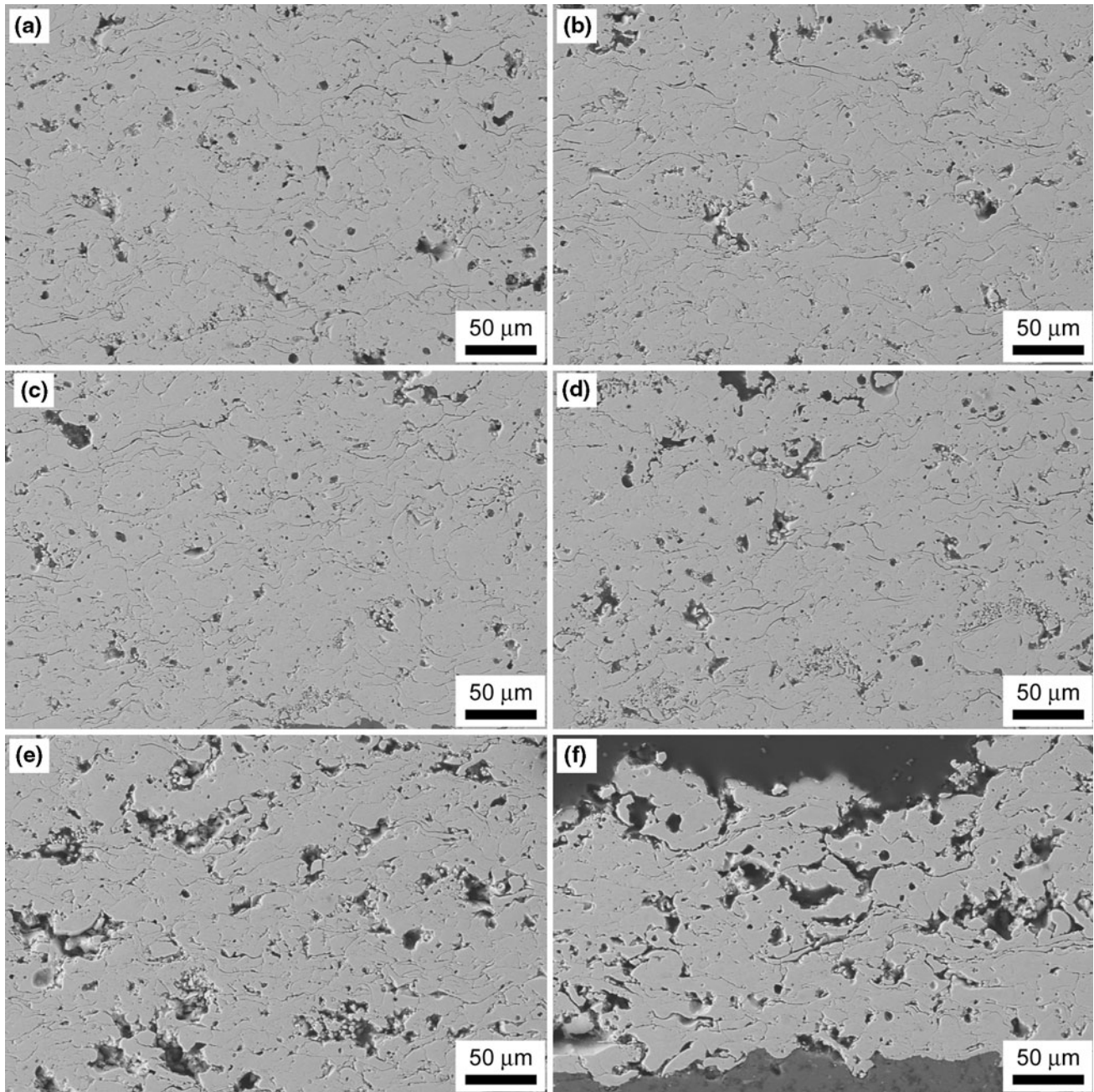
Fig. 3 Backscattered electron images of the cross sections of YSZ coatings deposited at the powder feed rate R_f of (a) 15 g/min, (b) 30 g/min, (c) 45 g/min, and (d) 60 g/min at the standard spray distance $x = 100$ mm. Those of R_f (e) 15 g/min and (f) 60 g/min at a longer spray distance $x = 150$ mm are also shown. Hollow spherical powder of YSZ (10-75 μm) was sprayed onto Al beams at 34 kW

Fig. 10 (Ref 30). As the splat bonding occurs during this bead formation, the surface temperature where the particle plume is impinging (referred to as the local deposition temperature) is more descriptive of the phenomena involved than the macroscopic average substrate temperature. The local deposition temperature is expected to be much higher than the measured substrate temperature. At a higher deposition rate, heat input from the particle plume per unit area per unit time will also become larger, resulting in a higher local deposition temperature.

For simplicity, an equivalent thickness that is equal to the average thickness of the bead, h_{eq}, is introduced instead of considering the shape of the bead. This h_{eq} can be calculated by

$$h_{eq} = \frac{R_f \eta}{PUW_z}, \tag{Eq 5}$$

where P and W_z are the coating density and the particle plume width perpendicular to the robot-scanning direction, respectively. The time to move by the width of the
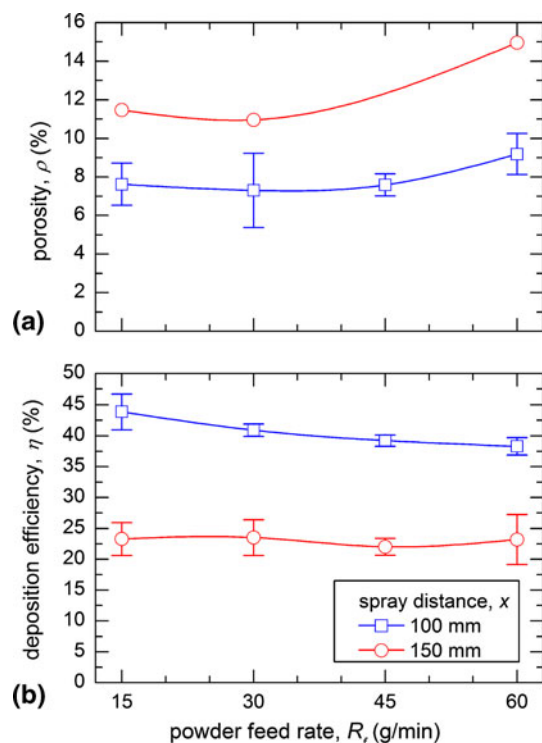
Fig. 4 Effect of the powder feed rate R_f on (a) the porosity ρ and (b) the deposition efficiency η of YSZ coatings deposited at the spray distances $x = 100$ and 150 mm. The value of ρ is calculated from backscattered electron images of cross sections of the coatings using an image analysis. The error bars for ρ at $x = 100$ mm are the standard deviation of six images; those for η at $x = 100$ mm are the standard deviation of six samples, while those at $x = 150$ mm that of 4-5 samples. Hollow spherical powder of YSZ (10-75 μm) was sprayed onto Al beams at 34 kW (Color online)

particle plume along the robot-scanning direction (W_y), Δt, is given by

$$\Delta t = \frac{W_y}{U}. \qquad (Eq\ 6)$$

Therefore, a deposition rate at a specific location (named a local deposition rate), R_{LD}, is given by

$$R_{LD} = \frac{h_{eq}}{\Delta t} = \frac{\eta}{W_y \cdot W_z \cdot P} R_f. \qquad (Eq\ 7)$$

An interval between successive depositions of splats at a same location, namely, a splat deposit interval Δt_{sp} can be calculated from R_{LD} by

$$\Delta t_{sp} = \frac{h_{sp}}{R_{LD}}, \qquad (Eq\ 8)$$

where h_{sp} is the average thickness of splats. As the splat deposit interval is shorter, a subsequent splat will form on a previously deposited splat which will increase the local temperature. This number can thus be used as an indicator to represent the local deposition temperature.

Note that the local deposition rate does not contain a term related to the robot speed; i.e., the local deposition
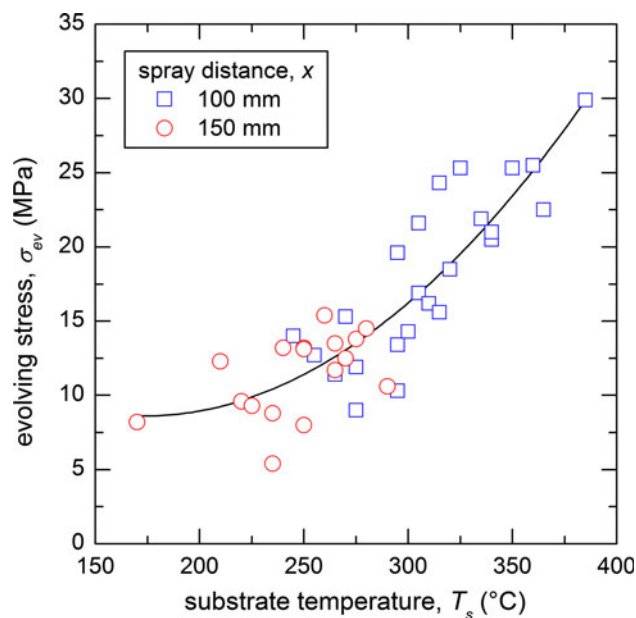

Fig. 5 Effect of substrate temperature T_s on evolving stress σ_{ev}. Data at two spray distances: standard ($x = 100$ mm) and longer ones ($x = 150$ mm) are plotted. Hollow spherical powder of YSZ (10-75 μm) was sprayed onto Al beams 2.4 mm thick at 34 kW (Color online)
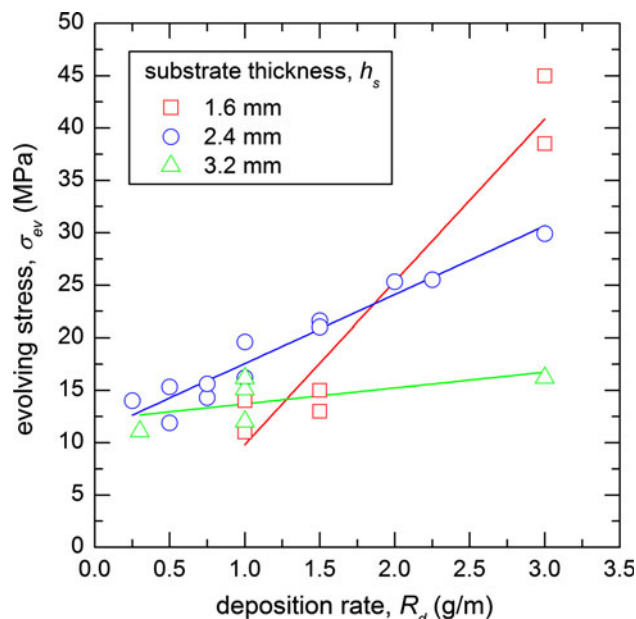

Fig. 6 Effect of substrate thickness h_s on evolving stress σ_{ev}. Hollow spherical powder of YSZ (10-75 μm) was sprayed at 34 kW on Al beams of which thickness was h_s at the spray distance of $x = 100$ mm (Color online)

rate is mainly determined by the powder feed rate and independent of the robot speed. Figure 11 shows the splat deposit interval that was calculated from Eq 8. Here, $W_y = W_z = 20$ mm and $h_{sp} = 1$ μm were assumed. The values of η and P were post-determined from coating weight
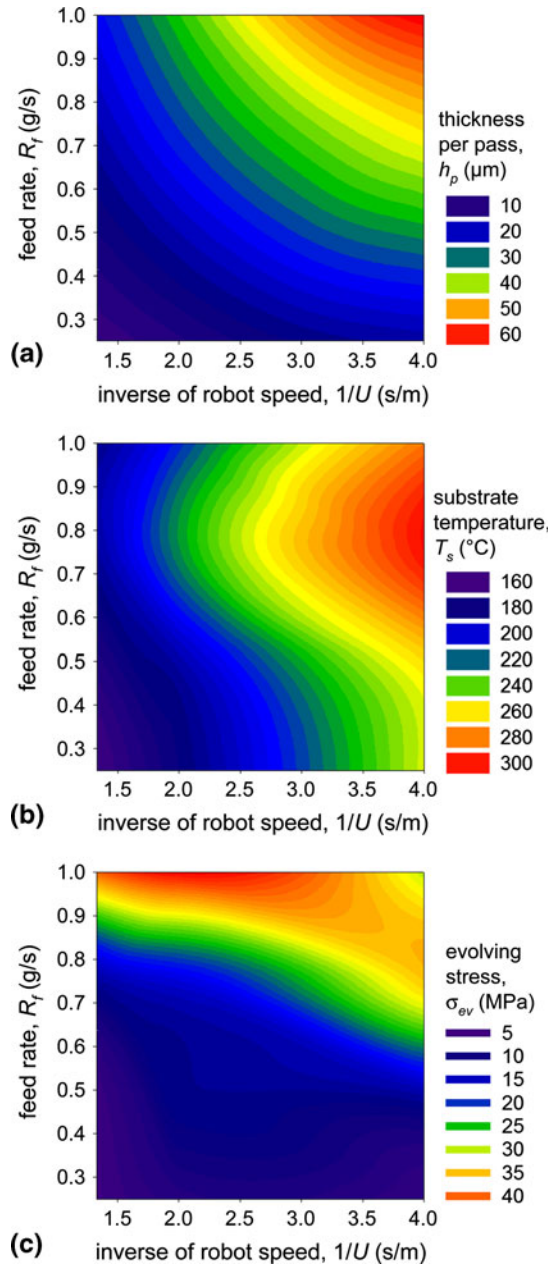
Fig. 7 Two-dimensional maps of (a) thickness per pass, h_p, (b) substrate temperature T_s, and (c) evolving stress σ_{ev} in powder feed rate R_f-robot speed U space. Hollow spherical powder of YSZ (10-75 μm) was sprayed onto Al beams 1.6 mm thick at 34 kW at the spray distance of $x = 100$ mm. The data of h_p are interpolated with that of 2.4 mm beams (Color online)

and thickness by definitions used in our previous work (Ref 4). Figure 11 clearly shows that the splat deposit interval is mainly governed by the powder feed rate.

Finally, the evolving stress is re-plotted against the substrate temperature and the local deposition rate in Fig. 12. The evolving stress tends to have increased with the increased substrate temperature and local deposition rate. Assuming that the effect of the local deposition rate on the evolving stress is attributed to a rise in the local
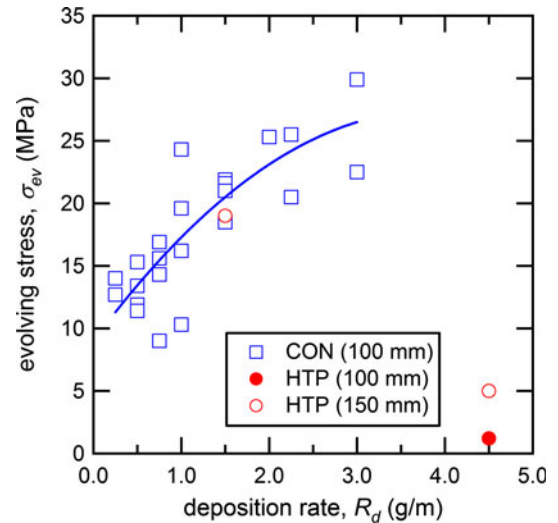

Fig. 8 Evolving stress of YSZ coatings deposited with a HTP plasma torch. Hollow spherical powder (10-75 μm) is sprayed onto a Ni-base superalloy beam 1.6 mm thick at 50 kW. Two spray distances $x = 100$ and 150 mm are shown. The powder feed rate was 90-135 g/min. For comparison, that with a CON plasma torch (re-plot of a data set of a spray distance of 100 mm in Fig. 2) is also shown (Color online)

deposition temperature, it can be estimated that the local deposition temperature within a range of this study was 50-100 °C higher than the substrate temperature. Figure 12 suggests the importance of the local deposition rate (inversely proportional to the splat deposit interval) on the evolving stress. Thus, these parameters will be good candidates to describe a process map for NPSPs.

Although the robot speed is not included in the local deposition rate, a "quiet" period emerging as the result of the robot-scanning pattern related to the sample geometry is worth to be mentioned. As the spray torch is not always on the specimen during deposition, a quiet period at which a bead is not formed can appear between and/or within spray passes. For example, when a beam such as ICP beams in this study is coated, as the robot-scanning length is usually taken longer than the beam length, the quiet period can go up to 70% of the spray time, resulting in cooling effects to the specimen. Meanwhile, when a cylindrical specimen is coated, the spray torch can always be on the specimen. In this case, the quiet period is zero, which can lead to a higher deposition temperature. Therefore, the resulting microstructure can be different despite of the same deposition rate. This concept is actually taken into account in our simulation previously reported (Ref 27), but is a subject of further experimental investigation.

4.2 Two Regimes for Stress Evolutions and Applicable Limitations

The decrease in the particle temperature and velocity at higher feed rates at constant power conditions due to the powder loading effect usually causes an increase in the coating porosity and/or poor bonding of splats. Thus, it is
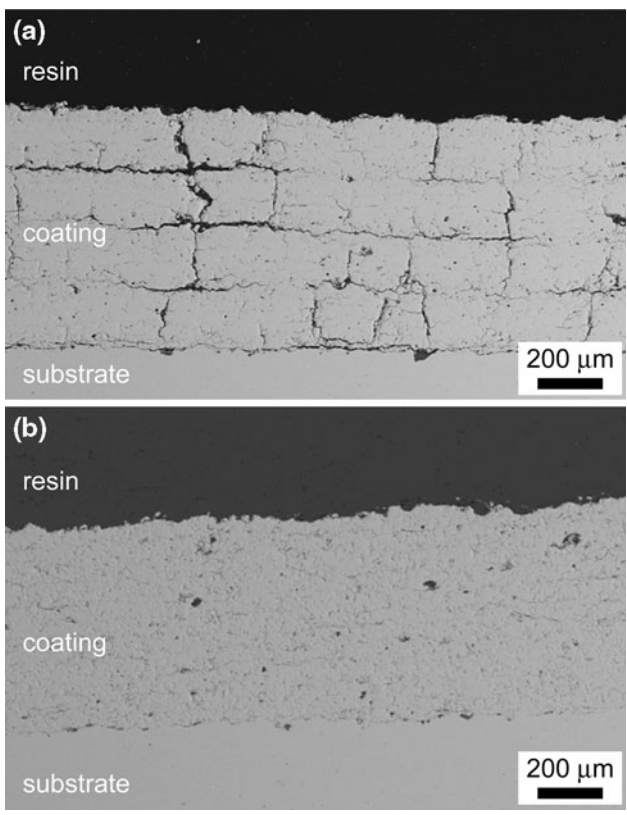
Fig. 9 Backscattered electron images of the cross sections of YSZ coatings deposited with a HTP plasma torch (a) at a high deposition rate $R_d = 4.5$ g/m and a spray distance $x = 100$ mm and (b) at a CON deposition rate $R_d = 1.5$ g/m and $x = 150$ mm. Hollow spherical powder (10-120 μm) was sprayed onto a Ni-base superalloy beam 1.6 mm thick at 50 kW. The evolving stress of these coatings is shown in Fig. 8
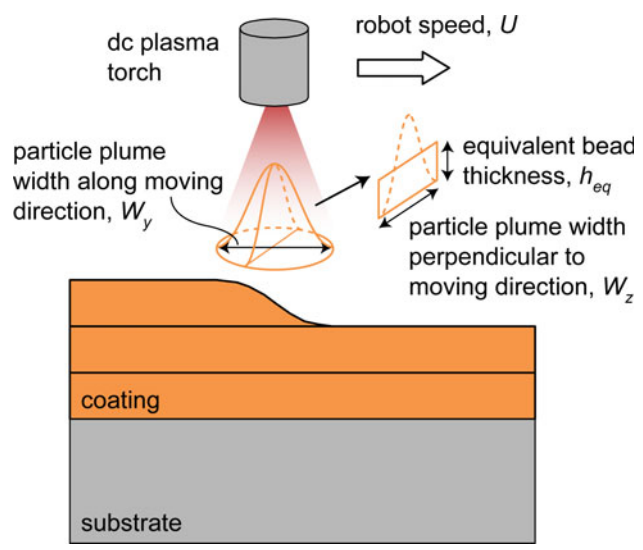

Fig. 10 Schematic of coating formation in plasma spraying to explain the concept of local deposition rate (Color online)

expected that the evolving stress becomes lower in terms of decreases in particle temperature and velocity with the powder feed rate. However, the evolving stress increased
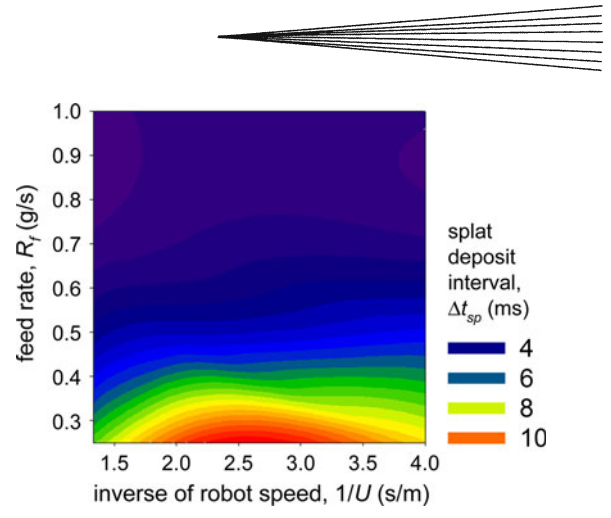

Fig. 11 Splat deposit interval Δt_{sp} as a function of powder feed rate R_f and robot speed U. Hollow spherical powder of YSZ (10-75 μm) was sprayed onto Al beams at 34 kW (Color online)
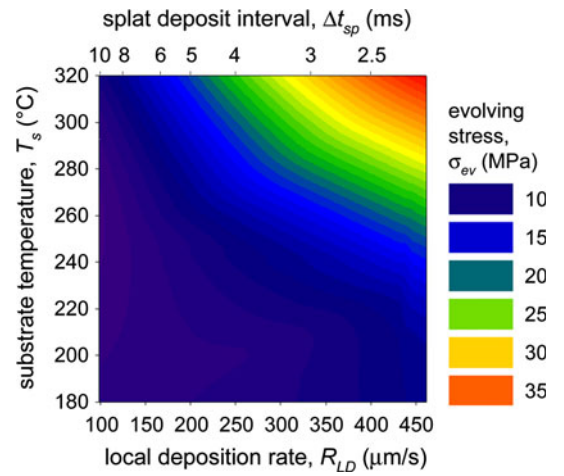

Fig. 12 Two-dimensional mapping of evolving stress (σ_{ev}) in substrate temperature (T_s)-local deposition rate (R_{LD}) space. Splat deposit interval (Δt_{sp}) is also shown, assuming the average splat thickness of 1 μm. Hollow spherical powder of YSZ (10-75 μm) was sprayed onto Al beams 1.6 mm thick at 34 kW (Color online)

with the powder feed rate within a range of this study. This fact implies that the evolving stress could be significantly higher if the powder feed rate were increased with keeping the particle temperature the same. Therefore, the intrinsic effect of the powder feed rate on the stress evolution will be stronger than the result shown in this study if the powder loading effect could be negligible. When the powder feed rate reaches a level of saturation (beyond a range of this study) in which the deposition efficiency will decrease significantly because of the powder loading rate, the evolving stress will experience a concomitant reduction.

We showed a concept of the local deposition rate (or the splat deposit interval), but the model shown above can be improved by taking PSPs into account. The proposed concept is based on values such as the deposition efficiency, the coating density, and the plume width used to calculate the local deposition rate. These post-determined
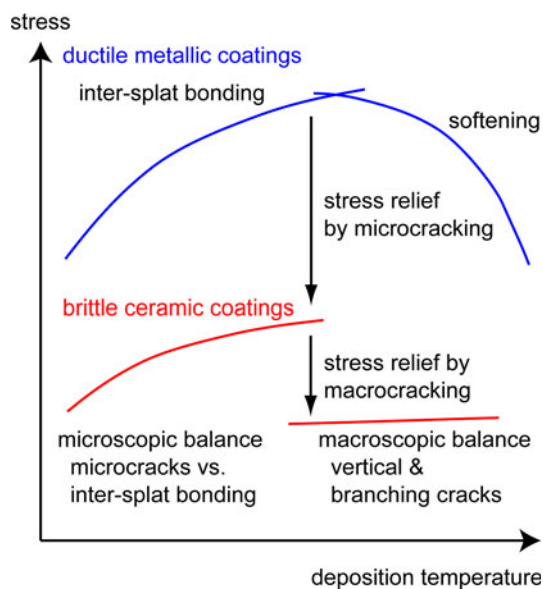
Fig. 13 Schematic diagram of the stress evolution in plasma-sprayed coatings. The case for ductile metallic coatings is adapted from a schematic diagram by Kuroda et al. (Ref 20) (Color online)

values can be refined by the inclusion of additional information from other models such as the melting index and splash criterion and/or by numerical simulations (Ref 31-36), making the calculation more precise and robust.

Summarizing this study, it will be possible to classify the stress evolutions in the plasma-sprayed brittle ceramic coatings such as YSZ into two regimes, as shown in Fig. 13. One is a microscopic-balancing regime in which the evolving stress increases with the deposition temperature. This local deposition temperature can be varied with the deposition rate. Here, the quenching stress is relieved in part by microcracking of individual splats, which causes the evolving stress to be lower compared to that of ductile metallic coatings as reported by Kuroda et al. (Ref 20). Above a certain threshold, coatings tend to have macroscopic vertical cracks as well as branching cracks to relief the stress (macroscopic-balancing regime). This is in contrast to the case of metallic coatings in which the stress relief occurred by creeping or plastic deformation above a softening point (Ref 20). More experimental data including other ceramic materials will be needed for quantitative understandings of this transition.

5. Conclusion

In this article, we have studied the effect of the deposition rate on the stress evolution of plasma-sprayed YSZ coatings by varying the powder feed rate and the robot-scanning speed. The main conclusions of this study are derived as follows:

(1) The evolving stress increases with the deposition rate, i.e., with the powder feed rate or with the inverse of the robot-scanning speed within a range in which the powder loading effect is not significant. This tendency is more obvious at a shorter spray distance. An increase in the deposition temperature with the deposition rate is a primary factor to the effect of the deposition rate. At a further high deposition rate using a HTP plasma torch, vertical cracks as well as branching cracks can be induced, resulting in lowering of the evolving stress.

(2) The effect of the powder feed rate on the stress evolution tends to be greater than that of the robot-scanning speed. This phenomenon can be explained by an introduction of the local deposition rate and the local deposition temperature. Impact intervals of successive splat particles (the inverse of the local deposition rate) become shorter with the powder feed rate, but are independent of the robot-scanning speed. Therefore, the local deposition temperature where the particle plume is impinging can be increased more with the increased powder feed rate than with the decreased robot-scanning speed, resulting in generation of a higher evolving stress.

(3) The local deposition rate and deposition temperature can be representative parameters of the NPSPs. By coupling these parameters to the PSPs such as particle temperature and velocity (or melting index and the Reynolds number at impact), a more robust process map method will be available.

References

1. A.A. Kulkarni, A. Goland, H. Herman, A.J. Allen, J. Ilavsky, G.G. Long, C.A. Johnson, and J.A. Ruud, Microstructure-Property Correlations in Industrial Thermal Barrier Coatings, *J. Am. Ceram. Soc.*, 2004, **87**(7), p 1294-1300
2. A. Vaidya, V. Sirinivasan, T. Streibl, M. Friis, W. Chi, and S. Sampath, Process Maps for Plasma Spraying of Yttria-Stabilized Zirconia: An Integrated Approach to Design, Optimization and Reliability, *Mater. Sci. Eng. A*, 2008, **497**(1-2), p 239-253
3. T. Yoshida, T. Okada, H. Hamatani, and H. Kumaoka, Integrated Fabrication Process for Solid Oxide Fuel Cells Using Novel Plasma Spraying, *Plasma Sources Sci. Technol.*, 1992, **1**(3), p 195-201
4. K. Shinoda, Y. Tan, and S. Sampath, Powder Loading Effects of Yttria-Stabilized Zirconia in Atmospheric dc Plasma Spraying, *Plasma Chem. Plasma Process.*, 2010, **30**(6), p 761-778
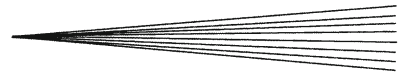
5. M. Friis, C. Persson, and J. Wigren, Influence of Particle In-flight Characteristics on the Microstructure of Atmospheric Plasma Sprayed Yttria Stabilized ZrO$_2$, *Surf. Coat. Technol.*, 2001, **141**(2-3), p 115-127

6. M. Prystay, P. Gougeon, and C. Moreau, Structure of Plasma-Sprayed Zirconia Coatings Tailored by Controlling the Temperature and Velocity of the Sprayed Particles, *J. Therm. Spray Technol.*, 2001, **10**(1), p 67-75

7. K. Shinoda, H. Murakami, S. Kuroda, K. Takehara, and S. Oki, In Situ Visualization of Impacting Phenomena of Plasma-Sprayed Zirconia: From Single Splat to Coating Formation, *J. Therm. Spray Technol.*, 2008, **17**(5-6), p 623-630

8. S. Sampath, V. Srinivasan, A. Valarezo, A. Vaidya, and T. Streibl, Sensing, Control, and in Situ Measurement of Coating Properties: An Integrated Approach Toward Establishing Process-Property Correlations, *J. Therm. Spray Technol.*, 2009, **18**(2), p 243-255

9. J. Colmenares-Angulo, K. Shinoda, T. Wentz, W. Zhang, Y. Tan, and S. Sampath, On the Response of Different Particle State Sensors to Deliberate Process Variations, *J. Therm. Spray Technol.*, 2011, **20**(5), p 1035-1048

10. S. Kuroda and T.W. Clyne, The Quenching Stress in Thermally Sprayed Coatings, *Thin Solid Films*, 1991, **200**(1), p 49-66

11. L. Bianchi, P. Lucchese, A. Denoirjean, P. Fauchais, and S. Kuroda, Evolution of Quenching Stress During Ceramic Thermal Spraying with Respect to Plasma Parameters, Advances in Thermal Spray Science & Technology, *Proceedings of the 8th National Thermal Spray Conference*, September 11-15, 1995 (Houston, TX), C.C. Berndt and S. Sampath, Ed., ASM International, Materials Park, OH, 1995, p 267-271

12. A.C. Leger, G. Delluc, A. Haddadi, P. Fauchais, and F. Nardou, Residual Stress Measurement During Plasma Spraying of Alumina or Zirconia and Comparison with a 1D Model, *High Temp. Mater. Process*, 1998, **2**, p 339-357

13. J. Matejicek and S. Sampath, In Situ Measurement of Residual Stresses and Elastic Moduli in Thermal Sprayed Coatings—Part 1: Apparatus and Analysis, *Acta Mater.*, 2003, **51**(3), p 863-872

14. S. Sampath, X. Jiang, A. Kulkarni, J. Matejicek, D.L. Gilmore, and R.A. Neiser, Development of Process Maps for Plasma Spray: Case Study for Molybdenum, *Mater. Sci. Eng. A*, 2003, **348**(1-2), p 54-66

15. N. Elkaddah, J. McKelliget, and J. Szekely, Heat-Transfer and Fluid-Flow in Plasma Spraying, *Metall. Trans. B*, 1984, **15**(1), p 59-70

16. X.C. Zhang, M. Watanabe, H. Murakami, and S. Kuroda, Relaxation of Compressive Residual Stress in Grit Blasted Substrate Due to Annealing Effect During Preheating and Spray Processes, *Proceedings of the 4th Asian Thermal Spray Conference*, October 22-24, 2009 (Xi'an, China), 2009

17. A. Valarezo, G. Bolelli, W.B. Choi, S. Sampath, V. Cannillo, L. Lusvarghi, and R. Rosa, Damage Tolerant Functionally Graded WC-Co/Stainless Steel HVOF Coatings, *Surf. Coat. Technol.*, 2010, **205**(7), p 2197-2208

18. A. Valarezo, W.B. Choi, W. Chi, A. Gouldstone, and S. Sampath, Process Control and Characterization of NiCr Coatings by HVOF-DJ2700 System: A Process Map Approach, *J. Therm. Spray Technol.*, 2010, **19**(5), p 852-865

19. S. Takeuchi, M. Ito, and K. Takeda, Modeling of Residual-Stress in Plasma-Sprayed Coatings—Effect of Substrate Temperature, *Surf. Coat. Technol.*, 1990, **43-4**(1-3), p 426-435

20. S. Kuroda, T. Dendo, and S. Kitahara, Quenching Stress in Plasma-Sprayed Coatings and Its Correlation with the Deposit Microstructure, *J. Therm. Spray Technol.*, 1995, **4**(1), p 75-84

21. Y.-Z. Xing, C.-J. Li, C.-X. Li, and G.-J. Yang, Relationship Between the Interlamellar Bonding and Properties of Plasma-Sprayed Y$_2$O$_3$-ZrO$_2$ Coatings, *Thermal Spray 2009: Proceedings of the International Thermal Spray Conference*, B.R. Marple, M.M. Hyland, Y.-C. Lau, C.-J. Li, R.S. Lima, and G. Montavon, Ed., ASM International, Materials Park, OH, 2009, p 939-944

22. V. Srinivasan, M. Friis, A. Vaidya, T. Streibl, and S. Sampath, Particle Injection in Direct Current Air Plasma Spray: Salient Observations and Optimization Strategies, *Plasma Chem. Plasma Process.*, 2007, **27**(5), p 609-623

23. G. Dwivedi, T. Wentz, S. Sampath, and T. Nakamura, Assessing Process and Coating Reliability Through Monitoring of Process and Design Relevant Coating Properties, *J. Therm. Spray Technol.*, 2010, **19**(4), p 695-712

24. G.G. Stoney, The Tension of Metallic Films Deposited by Electrolysis, *Proc. R. Soc. Lond.*, 1909, **A82**(553), p 172-175

25. S.C. Sharma, Effect of Albite Particles on the Coefficient of Thermal Expansion Behavior of the Al6061 Alloy Composites, *Metall. Mater. Trans. A*, 2000, **31**(3), p 773-780

26. Y. Liu, T. Nakamura, V. Srinivasan, A. Vaidya, A. Gouldstone, and S. Sampath, Non-Linear Elastic Properties of Plasma-Sprayed Zirconia Coatings and Associated Relationships with Processing Conditions, *Acta Mater.*, 2007, **55**(14), p 4667-4678

27. T. Nakamura and Y.J. Liu, Determination of Nonlinear Properties of Thermal Sprayed Ceramic Coatings Via Inverse Analysis, *Int. J. Solids Struct.*, 2007, **44**(6), p 1990-2009

28. C.A. Klein, How Accurate Are Stoney's Equation and Recent Modifications, *J. Appl. Phys.*, 2000, **88**(9), p 5487-5489

29. S. Sampath, X.Y. Jiang, J. Matejicek, A.C. Leger, and A. Vardelle, Substrate Temperature Effects on Splat Formation, Microstructure Development and Properties of Plasma Sprayed Coatings Part I: Case Study for Partially Stabilized Zirconia, *Mater. Sci. Eng. A*, 1999, **272**(1), p 181-188

30. M.I. Boulos, P. Fauchais, and J. Heberlein, *Understanding and Improving Your Thermal Spray Processes, a Lecture Note in International Thermal Spray Conference 2004*. 2004, Osaka

31. H.B. Xiong, L.L. Zheng, L. Li, and A. Vaidya, Melting and Oxidation Behavior of In-flight Particles in Plasma Spray Process, *Int. J. Heat Mass Transf.*, 2005, **48**(25-26), p 5121-5133

32. R. Ghafouri-Azar, J. Mostaghimi, and S. Chandra, Modeling Development of Residual Stresses in Thermal Spray Coatings, *Comput. Mater. Sci.*, 2006, **35**(1), p 13-26

33. R. Dhiman, A.G. McDonald, and S. Chandra, Predicting Splat Morphology in a Thermal Spray Process, *Surf. Coat. Technol.*, 2007, **201**(18), p 7789-7801

34. D. Wroblewski, O. Ghosh, A. Lum, D. Willoughby, M. VanHout, K. Hogstrom, S.N. Basu, and M. Gevelber, Modeling and Parametric Analysis of Plasma Spray Particle State Distribution for Deposition Rate Control, *ASME Conference Proceedings: ASME 2008 International Mechanical Engineering Congress and Exposition* (Boston, MA), ASME, 2008, p 453-460

35. V. Srinivasan and S. Sampath, Estimation of Molten Content of the Spray Stream from Analysis of Experimental Particle Diagnostics, *J. Therm. Spray Technol.*, 2010, **19**(1), p 476-483

36. S.N. Basu, G. Ye, M. Gevelber, and D. Wroblewski, Microcrack Formation in Plasma Sprayed Thermal Barrier Coatings, *Int. J. Refract. Met. Hard Mater.*, 2005, **23**(4-6), p 335-343